PCCP

Accepted Manuscript

ROYAL SOCIETY OF CHEMISTRY

www.rsc.org/pccp

Physical Chemistry Chemical Physics
CREATED USING THE RSC LaTeX PCCP ARTICLE TEMPLATE – SEE www.rsc.org/electronicfiles FOR DETAILS
ARTICLE TYPE www. rsc.org/xxxxxx | XXXXXXXX

Computational Assignment of Redox States to Coulomb Blockade Diamonds

Stine T. Olsen,[a] Vaida Arcisauskaite,[b] Thorsten Hansen,*[a c] Jacob Kongsted,[d] and Kurt V. Mikkelsen[a]

Received Xth XXXXXXXXXX 20XX, Accepted Xth XXXXXXXXX 20XX
First published on the web Xth XXXXXXXXXX 200X
DOI: 10.1039/b000000x

With the advent of molecular transistors, electrochemistry can now be studied at the single-molecule level. Experimentally, the redox chemistry of the molecule manifests itself as features in the observed Coulomb blockade diamonds. We present a simple theoretical method for explicit construction of the Coulomb blockade diamonds of a molecule. A combined quantum mechanical/molecular mechanical method is invoked to calculated redox energies and polarizabilities of the molecules, including the screening effect of the metal leads. This direct approach circumvent the need for explicit modelling of the gate electrode. From the calculated parameters the Coulomb blockade diamonds are constructed using simple theory. We offer a theoretical tool for assignment of Coulomb blockade diamonds to specific redox states in particular, and study of chemical details in the diamonds in general. With the ongoing experimental developments of molecular transistor experiments, our tool could find use in molecular electronics, electrochemistry, and electrocatalysis.

1 Introduction

The propensity of a molecule to accept or donate charge determines much of its chemistry, and with the advent of molecular single-electron transistors it is now possible to probe electrochemical processes at the single-molecule level. In this work, we demonstrate direct quantum chemical calculations of the redox state energies of a single molecule in the electrostatic environment of a molecular transport junction, and reconstruct the characteristic Harlequin pattern of Coulomb blockade diamonds observed in single-molecule transistor experiments [1–10].

The experimental realization of molecular transport junctions, with a molecule bridging two metallic electrodes, has made the study of molecular electronic processes possible at the single molecule level. In the regime of weak molecule-electrode coupling the charge on the molecule fluctuates under an applied bias voltage, causing electrochemistry of a single molecule. Under favourable experimental conditions the molecule responds to the potential of a third - gate - electrode. This can occur in solution in electrochemical STM or break-junction experiments, or it can occur in vacuum, with the molecule suspended as the active component in a three terminal device, usually fabricated using lithographic techniques. This is the setup inherited from mesoscopic physics, where transport through a quantum dot enters the Coulomb blockaded regime when the charging energy of the dot ΔE – the energy difference between two redox states – exceeds the state broadening caused by the coupling to the electrodes, $\Delta E > \Gamma$, and temperature $\Delta E \gg k_B T$. If the conductance is plotted as a function of gate voltage and bias voltage the characteristic Harlequin pattern of Coulomb blockade diamonds emerges. Each diamond indicates a region where current is suppressed, and the quantum dots remains in a specific charge state.

In the new millennium Coulomb Blockade diamonds have been observed in increasingly smaller systems such as carbon nano-tubes [11], and individual molecules [1–4]. In molecular transistors, chemical features begin to appear in the harlequin pattern, such as non-uniform ionization energies and vibrational sidebands. Kondo physics also appears in molecular transistors [5,12,13].

A direct quantum chemical approach for calculating the energies and polarizabilities of a range of redox states of a desired molecular wire is presented. We calculate the redox energies of the molecule directly, thus circumventing the need for explicit modelling of a third electrode. With the semi-classical modelling inherited from mesoscopic physics Coulomb blockade diamonds are reconstructed. Including the molecular polarizability allows the molecular charge density to respond the applied bias. We can now investigate how chemical features, such as configuration, binding groups, and redox state, of a molecule manifest themselves in the Coulomb blockade dia-

[a] *Department of Chemistry, University of Copenhagen, Universitetsparken 5, 2100 Copenhagen Ø, Denmark*
[b] *Department of Chemistry, Oxford University, South Parks Road, Oxford OX1 3QZ, United Kingdom*
[c] *Department of Chemical Physics, Lund University, Box 124, SE 221 00, Lund, Sweden*
[d] *Department of Physics, Chemistry and Pharmacy, University of Southern Denmark, Campusvej 55, 5230 Odense M, Denmark*
∗ *thorsten@chem.ku.dk*

monds.

In contrast to the coherent transport regime where computational studies, often based on non-equilibrium Green's functions transport theory combined with electronic structure calculations at the density functional theory (DFT) level, are abundant, genuine quantum chemical treatments of molecular transistors are largely absent from the literature. Theoretically constructed Coulomb blockade diamonds presented in the literature are often based on model Hamiltonians [14–17]. A few works present calculations using dielectric continuum models for the electrodes combined with quantum mechanical description of the molecule [18–20].

2 Electrostatics of a Molecular Transport Junction

A total hamiltonian, H, for a molecular transport junction is given as a sum of hamiltonians for the molecule, H^{mol}, the leads, H^{leads}, plus a term V that comprises electronic coupling and electrostatic interactions among the subsystems.

$$H = H^{mol} + H^{leads} + V \tag{1}$$

We restrict the treatment to the weak coupling regime, and thus consider the energetics of the system in the absence of electronic coupling. We can now focus on the molecule and represent the presence of the leads as exposure to an external electrostatic potential, $\phi^{ext}(\mathbf{r})$. We write an effective molecular hamiltonian as

$$H^{eff,mol} = H^{mol} + \int d\mathbf{r}\rho^{mol}(\mathbf{r})\phi^{ext}(\mathbf{r}), \tag{2}$$

where $\rho^{mol}(\mathbf{r})$ is the molecular charge density. The total electrostatic potential, $\phi^{total}(\mathbf{r}) = \phi^{mol}(\mathbf{r}) + \phi^{ext}(\mathbf{r})$, fulfils the Poisson equation

$$\nabla^2\phi^{total}(\mathbf{r}) = -\frac{\rho^{mol}(\mathbf{r})}{\varepsilon(\mathbf{r})}, \tag{3}$$

where $\varepsilon(\mathbf{r})$ is the dielectric function, with the Dirichlet boundary conditions that the potential takes specified values ϕ_1 and ϕ_2 at the lead surfaces. A full-fledged numerical solution of this equation is beyond the scope of this work.

The external potential describes two physical effects: the polarization of the leads screening the molecular charge density and the applied bias. We write the external potential as a sum of two contributions,

$$\phi^{ext}(\mathbf{r}) = \phi^{pol}(\mathbf{r}) + \phi^{bias}(\mathbf{r}), \tag{4}$$

and invoke the linearity of the Poisson equation to solve two separate electrostatic problems. The zero-bias ($\phi_1 = \phi_2$) problem

$$\nabla^2(\phi^{mol}(\mathbf{r}) + \phi^{pol}(\mathbf{r})) = -\frac{\rho^{mol}(\mathbf{r})}{\varepsilon(\mathbf{r})}, \tag{5}$$

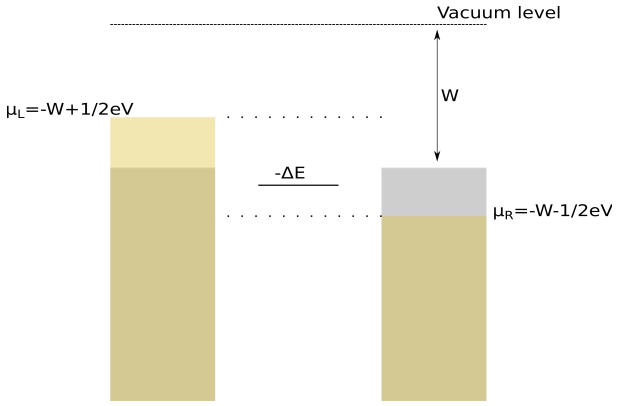

Fig. 1 Energetics of molecular transport junction. The grey area indicates the Fermi sea of the electrodes at zero bias, whereas the yellow areas show the Fermi sea under an applied bias. A molecular transistor is realized by introducing a third - gate - electrode which shifts the position of $-\Delta E$.

is solved using a quantum mechanical/molecular mechanical (QM/MM) approach described below. This calculation provides redox energies, E_q, and polarizabilities, α_q, of molecular states which are used to construct the Coulomb blockade diamonds of the molecular transistor.

The bias potential fulfils the Laplace equation, $\nabla^2\phi^{bias}(\mathbf{r}) = 0$, with Dirichlet boundary conditions such that $\phi_1 - \phi_2 = V$. For this work, we have chosen a simple electrode geometry to ensure an analytical solution of the Laplace equation. The shift of a molecular energy level with applied bias can be represented as

$$E_q(\phi^{bias}) - E_q = \int d\mathbf{r}\rho^{mol}(\mathbf{r},\phi^{bias})\phi^{bias}(\mathbf{r}), \tag{6}$$

where we include the dependence of the charge density on the bias. Expanding the potential as $\phi^{bias}(\mathbf{r}) \simeq \phi^{bias}(\mathbf{r}_0) + (\mathbf{r} - \mathbf{r}_0)\cdot\nabla\phi^{bias}(\mathbf{r}_0)$, we obtain

$$\begin{aligned}
&\int d\mathbf{r}\rho^{mol}(\mathbf{r},\phi^{bias})\phi^{bias}(\mathbf{r}) \\
&= \int d\mathbf{r}\rho^{mol}(\mathbf{r},\phi^{bias})\phi^{bias}(\mathbf{r}_0) + \int d\mathbf{r}\rho^{mol}(\mathbf{r},\phi^{bias})(\mathbf{r}-\mathbf{r}_0)\cdot\nabla\phi^{bias}(\mathbf{r}_0) \\
&= q\phi^{bias}(\mathbf{r}_0) + \mu(\mathbf{r}_0)\cdot\nabla\phi^{bias}(\mathbf{r}_0) \\
&= q\phi^{bias}(\mathbf{r}_0) - \mu(\mathbf{r}_0)\cdot\mathbf{F}(\mathbf{r}_0),
\end{aligned} \tag{7}$$

where $q = \int d\mathbf{r}\rho^{mol}(\mathbf{r},\phi^{bias})$ is the molecular charge and $\mu(\mathbf{r}_0) = \int d\mathbf{r}\rho^{mol}(\mathbf{r},\phi^{bias})(\mathbf{r}-\mathbf{r}_0)$ is the molecular dipole moment. The first term relates to gating, which is discussed below. The second term is the familiar expression for the energy of a dipole in an electric field $F(\mathbf{r}_0) = -\nabla\phi^{bias}(\mathbf{r}_0)$. This expression will be used below.

The energetics of a single-molecule transistor is illustrated in Figure 1. At zero bias, electrons exit or enter the gold leads

at an energy -W relative to vacuum, where W is the work function of the electrode which depends on the Fermi energy of the metal and the local geometry of the surface, which determines the surface charge distribution that the electron will move through. Experimentally, the local work function is accessible via two-photon photoemission spectroscopy, yet in this work we use a literature value representative of a [111] gold surface. For an electron to transfer from/to the Fermi surface of the lead to/from the molecule (or small quantum dot, where the level quantization is appreciable) the work function must match the electron affinity/ ionization potential of the molecule. We write

$$-W = -\Delta_q E \tag{8}$$

where $\Delta_q E = E_{q+1} - E_q > 0$. In a single-electron picture the IP/EA reduces to an orbital energy (of the HOMO/LUMO in the case of the neutral molecule), which motivates the short straight line in Figure 1.

A bias voltage applied across the molecule impacts both sides of equation 8. The chemical potential of the electrode shifts relative to each other. We assume that the voltage drop is divided equally between the two electrodes: $\mu_{L/R}(V) = -W \pm \frac{1}{2}eV$. As a consequence of the bias, the molecule is exposed to an electric field which depends on the electrode geometry. For simplicity, we assume that the molecule is located between two flat gold surfaces, and thus exposed to a homogenous electric field $F = V/d$, where d is the interelectrode distance. The applied field shifts the energy of the molecular states. We represent the molecule as a field dependent dipole, which is expanded to first order in the field $\mu(F) = -\frac{\partial E_q(F)}{\partial F} = \mu_q + \alpha_q F$. The field dependent energy reads:

$$E_q(F) = E_q - \int_0^F \mu_q(F')dF' = E_q - \mu_q F - \frac{1}{2}\alpha_q F^2 \tag{9}$$

The presence of a nearby gate electrode alters the electrostatic environment of the molecule. We shall adopt the approximation that molecule feels a constant potential that shifts linearly with the gate bias, V_g, thus $E_q(V_g) = E_q + qKV_g$. The constant K depends on the geometrical details of the setup and is not immediately accessible by experiment.

Taking bias voltage and gate voltage into account, the energy balance between two redox states is described by:

$$-W \pm \frac{1}{2}eV = -\Delta_q E + \Delta_q \mu \frac{V}{d} + \frac{1}{2}\Delta_q \alpha \frac{V^2}{d^2} - eKV_g \tag{10}$$

The solutions to this equation outline the Coulomb blockade diamonds. For each electrode we obtain a quadratic equation in eV for a total of four solutions, yet only two of these remain finite in the $\Delta_q\alpha \to 0$ limit. Considering the left electrode ($\mu_L(V) = -W + \frac{1}{2}eV$) and solving for eV, we obtain:

$$eV = \frac{e^2d^2}{\Delta_q\alpha}\left(-\frac{\Delta_q\mu}{ed} + \frac{1}{2} \pm \sqrt{\left(\frac{\Delta_q\mu}{ed} - \frac{1}{2}\right)^2 - 2\frac{\Delta_q\alpha}{e^2d^2}\left(W - \Delta_q E - eKV_g\right)}\right) \tag{11}$$

where only the $+\sqrt{\cdots}$ term remains finite. In the computational work that we discuss below, no dipole moments in the interelectrode direction were obtained, and we set $\Delta_q\mu = 0$ for simplicity. The two surviving solutions are giving by:

$$V = \frac{d^2}{\Delta\alpha}\left(\pm\frac{1}{2}e \pm \sqrt{\frac{1}{2}e^2 + \frac{2\Delta\alpha}{d^2}\left(\Delta E - W + eKV_g\right)}\right), \tag{12}$$

which defines the two crossing lines outlining the adjacent edges of two neigboring diamonds. Thus, the zero bias crossover from one redox state to the next corresponds to the crossing point between two diamonds. For five redox states the diamonds appear in the order of $q = +1, 0, -1$ from left to right.

The height of the diamond is determined from the crossing point of the two diamond edges, each described by Eq. 12. In the limit of zero polarizability the height equals two times the addition energy:

$$E^{add,junc} = \frac{1}{e}(E_{q-1} + E_{q+1} - 2E_q) \tag{13}$$

A modelling strategy for the construction of Coulomb blockade diamonds has been presented, which allows investigations of specific molecules in junction.

3 Computational Strategy

A combined QM/MM approach is used to calculate the energies E_q and polarizabilities α_q of a range of redox states of 1,4-dithiol-benzene (OPV1) and 4,4'-dimercaptostilbene (OPV2). The molecule is treated quantum mechanically, and the electrodes are represented as two clusters of MM atoms that are assigned with atomic polarizabilities. Calculations were performed utilizing a damping mechanism between the MM induced dipole moments and a dampning of the QM electric field at the polarizable MM sites[21]. All numbers presented arise from fully self-consistent calculations. This way, the screening of molecular charge by polarization of the electrodes is included in the calculated redox energies E_q.

The molecular geometries were optimized in vacuum using DFT with the long-range-corrected exchange-correlation functional of CAM-B3LYP[22] with the correlation consistence basis sets cc-pVDZ and cc-pVTZ[23], referred to as DZ and TZ, respectively. The molecule faces the [111] surfaces of two hemispheres of gold that are cut from a bulk FCC crystal. Each hemisphere contains 85 atoms. The axis through the two sulphur atoms stand perpendicular to the gold surface, with a sulphur to surface distance of 1.58Å[24]. The full junction geometry is illustrated in Figure 2. The electronic energy and polarization was calculated at the DFT level utilizing the same functionals and basis set as for the vacuum calculations. The MM gold atoms were assigned a polarizability value of

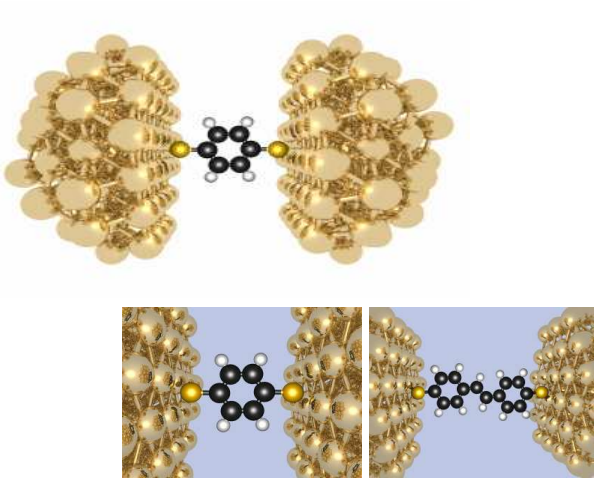

Fig. 2 Schematic representation of OPV1 and OPV2 sandwiched in the gold junction.

31.04 a.u.[25]. The polarization was determined in a fully self-consistent calculation. Calculations were performed for five redox states of the molecule with total charge ranging from -2e to 2e. The additional charge is added or subtracted to the QM part of the system. This represents a simple alternative to a more elaborate charge localization schemes such as constrained DFT. To construct the Coulomb blockade diamonds the parameters E_q and α_q obtained from the QM/MM calculations were inserted into to equation 12. For a more detailed description of the computational work our previous work can be consulted[26,27].

4 Results

Our systems of interest OPV1 and OPV2 are depicted in Figure 2. Total QM/MM energies for a series of redox states of both systems are displayed in Tables 1 and 2. The total energy of the molecule calculated in the absence of leads are denoted E^{vac}. $E^{rel,vac}$ denotes the same energies shifted by a constant. The shift in total molecular energy as the molecules are immersed in the transport junctions is denoted E^{pol}.

The total energies of the molecules in the junction, shifted linearly for convenience, $E^{rel,junc} = E^{rel,vac} + E^{pol}$ is depicted in Figure. 3. The minimum energies are found for anionic species. Evidently, the polarisation of gold is sufficient to stabilize additional electrons, presumably located at the sulphur atoms. The polarization energies by themselves are shown in Figure 4. The compliance of the values with a simple image charge model is illustrated by the inserted parabolas $E = -aQ^2$, where $a = 1$ for OPV1 and $a = 0.7$ for OPV2. We attribute the lower value of a for OPV2 to a delocalization of the additional charge, *i.e.* more charge is further away from the leads. As depicted in Figures 3 and 4 the above observations are true independent of basis set, albeit with minor differences in the energy values.

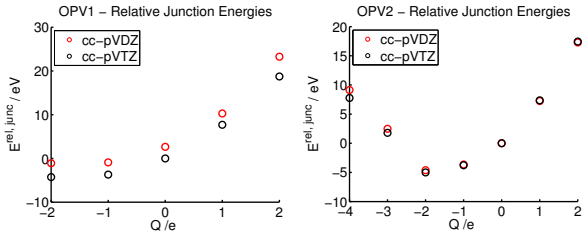

Fig. 3 Total energies, $E^{rel,junc} = E^{rel,vac} + E^{pol}$, of molecules OPV1 and OPV2.

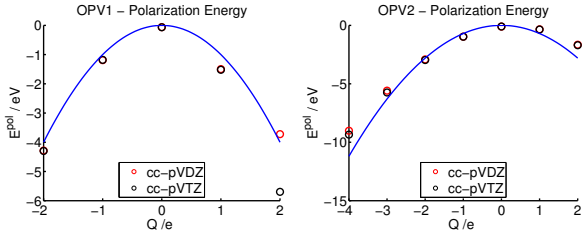

Fig. 4 Polarization energies for OPV1 and OPV2. A parabola $E = -aQ^2$ is inserted to guide the eye. We use $a = 1$ for OPV1 and $a = 0.7$ for OPV2.

The Harlequin pattern of Coulomb blockade diamonds depicted in Figures 5 and 6 are constructed using equation 12. This way the calculated redox energies are represented in a format that connects directly to experiment. Consequences of chemical variations on diamond features is apparent, and easy to recognize. The chemically similar molecules exhibit the same pattern of diamond sizes. For the TZ calculations the central diamonds are the largest, suggesting that the neutral species is most resilient towards charging. The diamonds plotted for OPV2 are smaller than the corresponding ones for OPV1, reflecting the smaller ionization potential and electron affinities of the larger conjugated molecule OPV2.

The addition energy, defined as $E^{add,junc}$, equals half of the height of the diamond. The calculated addition energies (equation 13) are tabulated in Tables 1 and 2. The relative reduction of diamond size induced by the leads ($(E^{add,vac} - E^{add,jun})/E^{add,vac}$) is denoted Diff. We interpret the smaller stabilization for the larger molecule as a consequence of larger delocalisation of the additional charge. Our reduction are smaller than estimates reported in the literature, suggesting that the geometries shown in Figures 2 are not representative of all experiments[3,28].

When the molecular polarizability is included in equation 12, the diamond edges acquire curvature. We observe

both convex and concave diamonds. The diamond sizes remain largely unaltered by the inclusion of polarizability, supporting the interpretation that image charge effects are dominating as opposed to Stark shift of the molecular levels. Many experimental Coulomb blockade diamonds appear to have straight edges, suggesting that polarisation of the molecule is not a major effect. In some experiments, however, the diamonds do exhibit curved edges, and molecular polarization offers one mechanism for this. The above observations concerning the Coulomb blockade diamonds are again independent of basis set.

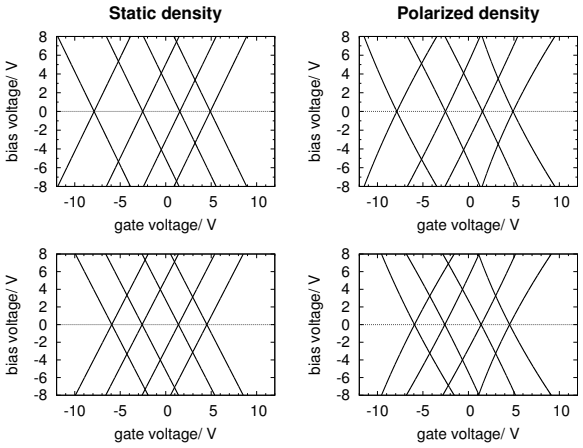

Fig. 5 Harlequin patterns of the Coulomb blockade diamonds for OPV1. The columns show patterns for static ($\Delta\alpha = 0$) and polarized densities. The rows show patterns for basis sets DZ and TZ.

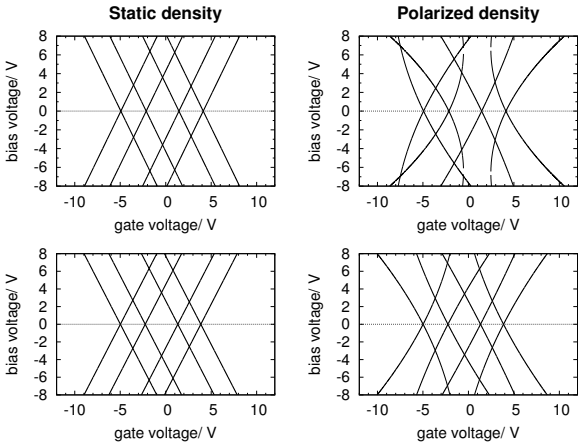

Fig. 6 Harlequin patterns of the Coulomb blockade diamonds for OPV2. The columns show patterns for static ($\Delta\alpha = 0$) and polarized densities. The rows show patterns for basis sets DZ and TZ.

5 Conclusion

We have developed a computational strategy for investigating single-molecule transistors, by explicitly constructing the harlequin pattern of Coulomb blockade diamonds for direct comparison with experiment. The key advantage of our QM/MM approach is its inherent ability to localize additional electrons on the molecule. More elaborate schemes of electron localization, such as e.g. constrained DFT[29], are yet to be applied to molecular transistors.

The direct calculation of redox energies circumvent the need for explicit modelling of a third electrode. More elaborate treatments of the electrostatics which obtain the electric field by solving the Poisson equation do, in principle, offer a better description of the field[20,30]. Experimentally, however, the assumption of linear response to the gate is well justified, thus a better description of the field will be particularly interesting for modelling the shapes of the source and drain electrodes.

In conclusion, our simple and inexpensive approach offers a window into the electrochemistry of a single molecule. We believe, it will find use in molecular electronics, electrochemistry, electrocatalysis, and related fields.

Acknowledgement

VA thanks Dr. Alytis Gruodis and Dr. Kestutis Aidas for fruitful discussions and the European Physical Society for student's mobility grant (coordinator Prof. Gintaras Dikcius and Prof. Izabela Sosnowska). TH thanks the Swedish Research Council (VR) and the Lundbeck Foundation. JK thanks the Danish Councils for undependent research, the Lundbeck foundation, the Villum foundation, and the Danish e-Infrastructure Coorporation for financial support. KVM thanks the Danish Research Council, Center for Exploitation of Solar Energy and Danish Center for Scientific Computing.

References

1 A. Danilov, S. Kubatkin, S. Kafanov, P. Hedegård, K. Month-Poulsen and T. Bjørnholm, *Nano Lett.*, 2008, **8**, 1.
2 E. A. Osorio, T. Bjørnholm, J.-M. Lehn, M. Ruben and H. S. J. van der Zant, *J. of Phys.*, 2008, **20**, year.
3 S. Kubatkin, A. Danilov, M. Hjort, C. J., J.-C. Bredas, N. Stuhr-Hansen, P. Hedegård and T. Bjørnholm, *Nature*, 2003, **425**, 698.
4 H. Park, J. Park, A. K. L. Lim, E. H. Anderson, A. P. Alivisatos and P. L. McEuen, *Nature*, 2000, **407**, 57.
5 W. Liang, M. P. Shores, M. Bockrath, J. R. Long and H. Park, *Nature*, 2002, **417**, 725.
6 A. Barreiro, H. S. J. van der Zant and L. M. K. Vandersypen, *Nano Lett.*, 2012, **12**, 6096.
7 H. S. J. van der Zant, Y.-V. Kervennic, M. Poot, K. O'Neill, Z. de Groot, J. M. Thijssen, H. B. Heersche, N. Stuhr-Hansen, T. Bjørnholm, D. Vanmaekelbergh, C. A. van Walree and L. W. Jenneskens, *Faraday Discuss.*, 2006, **131**, 347.

8 J. M. Thijssen and H. S. J. Van der Zant, *Phys. Status Solidi B*, 2008, **245**, 1455.
9 S. Sapmaz, P. Jarillo-Herrero, J. Kong, C. Dekker, L. P. Kouwenhoven and H. S. J. van der Zant, *Phys. Rev. B*, 2005, **71**, 153402.
10 J. S. Bunch, Y. Yaish, M. Brink, K. Bolotin and P. L. McEuen, *Nano Lett.*, 2005, **5**, 287.
11 J. Nygård, D. H. Cobden and P. E. Lindelof, *Nature*, 2000, **408**, 342.
12 L. H. Yu and D. Natelson, *Nano Lett.*, 2004, **4**, 79.
13 L. H. Yu and D. Natelson, *Nanotechnology*, 2004, **15**, S517.
14 E. Perfetto and G. Stefanucci, *Phys. Rev. B*, 2013, **88**, 245437.
15 G. Begemann, D. Darau, A. Donarini and M. Grifoni, *Phys. Rev. B*, 2008, **77**, 201406.
16 M. Esposito and M. Galperin, *Phys. Rev. B*, 2009, **79**, 205303.
17 J. P. Bergfield and C. A. Stafford, *Phys. Rev. B*, 2009, **79**, 245125.
18 R. Chowdhury, S. Adhikari and P. Rees, *Physica B*, 2012, **407**, 855.
19 H. Ying, W. Zhou, K. Chen and G. Zhou, *Comp Mater Sci*, 2014, **82**, 33.
20 K. Stokbro, *JPCC*, 2010, **114**, 20461.
21 V. Arcisauskaite, J. Kongsted, T. Hansen and K. V. Mikkelsen, *Chem. Phys. Letters*, 2009, **470**, 285.
22 T. Yanai, D. P. Tew and N. C. Handy, *Chem. Phys. Letters*, 2004, **393**, 51.
23 T. H. Dunning, *J. Chem. Phys.*, 1989, **90**, 1007–1023.
24 A. Bilic, J. R. Reimers and N. S. Hush, *J.Chem. Phys.*, 2005, **122**, 094708.
25 T. Hansen, T. Hansen, V. Arcisauskaite, K. V. Mikkelsen, J. Kongsted and V. Mujica, *J. Phys. Chem. C*, 2010, **114**, 20870.
26 S. T. Olsen, T. Hansen and K. V. Mikkelsen, *Theor. Chem. Acc.*, **130**, 839.
27 J. M. Olsen, K. Adias and J. Kongsted, *J. J. Chem. Theory. Comput.*, 2010, **6**, 3721.
28 P. Hedegård and T. Bjørnholm, *Chem. Phys.*, 2005, **319**, 350.
29 Q. Wu and T. Van Voorhis, *Phys. Rev. A*, 2005, **72**, 024502.
30 K. Kaasbjerg and K. Flensberg, *Phys. Rev. B*, 2011, **84**, 115457.

Table 1 OPV1 energies. Redox energies for molecule in vacuum and in junction (calculated from QM/MM). All energies are in units of eV.

Redox	Basis set	E^{pol}	E^{vac}	$E^{rel,vac}$	$E^{add,vac}$	$E^{add,jun}$	Diff
Q = 2	DZ	-3.723	-27929.359	26.912			
	TZ	-5.696[a]	-27931.911	24.359			
Q = 1	DZ	-1.496	-27944.562	11.709	6.141	5.350	13%
	TZ	-1.521	-27947.120	9.150	6.059	3.339	44%
Q = 0	DZ	-0.062	-27953.623	2.647	6.642	4.078	39%
	TZ	-0.066	-27956.270	0.000	6.564	3.994	39%
Q = -1	DZ	-1.191	-27956.043	0.228	5.319	3.354	37%
	TZ	-1.180	-27958.856	-2.586	5.133	3.130	39%
Q = -2	DZ	-4.285	-27953.144	3.127			
	TZ	-4.299	-27956.309	-0.038			

a: Calculation did not converge. B3LYP/cc-pVTZ value has been substituted. This explains the extreme basis set dependence.

Table 2 OPV2 energies. Redox energies for molecule in vacuum and in junction (calculated from QM/MM). All energies are in units of eV.

Redox	Basis set	E^{pol}	E^{vac}	$E^{rel,vac}$	$E^{add,vac}$	$E^{add,jun}$	Diff
Q = 2	DZ	-1.658	-36323.423	23.890			
	TZ	-1.698	-36328.282	19.031			
Q = 1	DZ	-0.341	-36334.771	12.542	3.8621	2.783	28%
	TZ	-0.359	-36339.705	7.608	3.8150	2.733	28 %
Q = 0	DZ	-0.103	-36342.258	5.055	4.7065	3.606	24 %
	TZ	-0.102	-36347.313	0	4.708	3.581	24 %
Q = -1	DZ	-0.966	-36345.038	2.275	3.750	2.6673	29%
	TZ	-0.971	-36350.213	-2.901	3.667	2.5407	31%
Q = -2	DZ	-2.912	-36344.067	3.246			
	TZ	-2.967	-36349.447	-2.135			